Acta Crystallographica Section D
Biological Crystallography
ISSN 0907-4449

Structural basis for the dephosphorylating activity of PTPRQ towards phosphatidylinositide substrates

Keum Ran Yu,[a] Young Jun Kim,[b] Suk-Kyeong Jung,[a] Bonsu Ku,[a] Hwangseo Park,[c] Sa Yeon Cho,[d] Hyeyun Jung,[a] Sang J. Chung,[e] Kwang Hee Bae,[a] Sang Chul Lee,[a] Bo Yeon Kim,[f] Raymond L. Erikson,[f] Seong Eon Ryu[g]* and Seung Jun Kim[a]*

[a]Medical Proteomics Research Center, Korea Research Institute of Bioscience and Biotechnology, 111 Gwahangno, Yuseong-gu, Daejeon 305-806, Republic of Korea, [b]Department of Applied Biochemistry, Konkuk University, Danwol-dong 322, Chungju, Chungbuk 380-701, Republic of Korea, [c]Department of Bioscience and Biotechnology, Sejong University, 98 Kunja-dong, Kwangjin-ku, Seoul 143-147, Republic of Korea, [d]College of Pharmacy, Chung-Ang University, Seoul 156-756, Republic of Korea, [e]Department of Chemistry, College of Natural Science, Dongguk University, 26, Pil-dong 3-ga, Jung-gu, Seoul 100-715, Republic of Korea, [f]Chemical Biology Research Center, Korea Research Institute of Bioscience and Biotechnology, 111 Gwahangno, Yuseong-gu, Daejeon 305-806, Republic of Korea, and [g]Department of Bio Engineering, Hanyang University, Seongdong-gu, Seoul 133-791, Republic of Korea

Correspondence e-mail: ryuse@hanyang.ac.kr, ksj@kribb.re.kr

Received 4 January 2013
Accepted 17 April 2013

PDB Reference: catalytic domain of PTPRQ, 4ikc

Unlike other classical protein tyrosine phosphatases (PTPs), PTPRQ (PTP receptor type Q) has dephosphorylating activity towards phosphatidylinositide (PI) substrates. Here, the structure of the catalytic domain of PTPRQ was solved at 1.56 Å resolution. Overall, PTPRQ adopts a tertiary fold typical of other classical PTPs. However, the disordered M6 loop of PTPRQ surrounding the catalytic core and the concomitant absence of interactions of this loop with residues in the PTP loop results in a flat active-site pocket. On the basis of structural and biochemical analyses, it is proposed that this structural feature might facilitate the accommodation of large substrates, making it suitable for the dephosphorylation of PI substrates. Moreover, subsequent kinetic experiments showed that PTPRQ has a strong preferences for PI(3,4,5)P_3 over other PI substrates, suggesting that its regulation of cell survival and proliferation reflects downregulation of Akt signalling.

1. Introduction

The tight control of phosphorylation or dephosphorylation at tyrosyl residues of proteins is a hallmark of signal transduction and is mainly governed by protein tyrosine kinases and protein tyrosine phosphatases (PTPs; EC 3.1.3.48). The dephosphorylation activities mediated by PTPs have been implicated in virtually all cellular processes, and inappropriate actions of PTPs cause various diseases (Tonks, 2006). A total of 38 human members of the classical PTP family (21 receptor-type PTPs and 17 nonreceptor-type PTPs) are known to exclusively dephosphorylate phosphorylated tyrosyl substrates (Alonso *et al.*, 2004). Classical PTPs share a catalytic module that is highly conserved in terms of three-dimensional structure and enzymatic mechanism. Briefly, the catalytic core of classical PTPs consists of a PTP loop (Cys-Ser-Xaa-Gly-Xaa-Gly-Arg-Thr/Ser) and a WPD loop. In the common active conformation the catalytic cysteine is located beneath the PTP loop and acts as a nucleophile. The amides of main-chain atoms and the guanidine group of the conserved arginine residue in the PTP loop point towards the interior of the loop, contributing to lowering the pK_a value of the catalytic cysteine. The WPD loop, in which aspartate acts as a general acid/base during catalysis, moves toward the PTP loop upon substrate binding (Barford *et al.*, 1994; Jia *et al.*, 1995). In addition to the catalytic core, the surrounding loops also play a role in catalysis. In particular, the M1 and M6 loops (Andersen *et al.*, 2001) render the catalytic pocket deep and narrow, resulting in a substrate preference for phosphotyrosine (pTyr) over phosphothreonine (pThr) or phosphoserine (pSer).

PTPRQ (PTP receptor type Q) is a member of the receptor-type PTP family that contains 18 extracellular fibronectin

domains and one cytoplasmic catalytic domain. Recent studies have shown that loss of the *PTPRQ* gene causes hearing loss with associated vestibular dysfunction (Goodyear *et al.*, 2012). Although the primary sequence of the catalytic domain of PTPRQ (PTPRQ-C) shows a high degree of similarity to those of other classical PTPs, PTPRQ displays unusual catalytic behaviour. Notably, PTPRQ has intrinsic dephosphorylating activity for various phosphatidylinositides (PIs) but not for phosphotyrosine substrates (Seifert *et al.*, 2003). Furthermore, PTPRQ negatively regulates cell proliferation and cell survival by lowering the level of phosphoinositol phosphates (PIPs; Oganesian *et al.*, 2003). One reason for this difference in dephosphorylating activity can be deduced from the primary sequences, namely that a strictly conserved aspartate in the WPD loop is changed to a glutamate in PTPRQ. Four catalytically active members of the classical PTP family (PTPRQ, PTPRU, PTPD1 and HDPTP) have a WPE motif instead of WPD in the human genome, but none has yet been structurally characterized. The fact that reverse mutation of glutamate to aspartate in the WPE motif causes PTPRQ to gain catalytic activity towards pTyr while losing activity towards PI substrates supports this notion. However, PTPRQ has only limited sequence homology to other PTPs such as PTEN (phosphatase and tensin homologue) and myotubularin phosphatases that are capable of dephosphorylating PIs (Alonso *et al.*, 2004). Moreover, the aspartate in the WPD loop is conserved in PTEN and is changed to an asparagine in myotubularin.

Understanding the origin of the PI-dephosphorylating activity of PTPRQ requires a structural and a subsequent biochemical investigation. Here, we report the crystal structure of PTPRQ-C at a resolution of 1.56 Å, which revealed that the M6 loop near the active site is disordered, resulting in a catalytic pocket that is flat on one side. Mutations that destabilize or delete the M6 loop showed a strong tendency to compromise the intrinsic dephosphorylating activity and slightly compromise (or leave unchanged) the dephosphorylating activity towards PI substrates, results that are consistent with structural observations.

2. Experimental procedures

2.1. Cloning, expression and purification

PTPRQ was cloned from human mesenchymal stem cells (MSCs) and subcloned into the pET28a vector carrying an N-terminal His tag using the primers 5′-GAG AGA TTA **CAT ATG** CCA ATA AGC AAG AAA-3′ and 5′-GTT AAC **GGA TCC** CTA GGG CTG ATT ACT TCC-3′ (sequences in bold denote *Nde*I and *Bam*HI sites used for cloning). PTPRQ-C (residues 2661–2948) was expressed in *Escherichia coli* BL21 (DE3) strain. PTPRQ-C single mutants (C2879S, E2785A, R2790A, E2847A and E2847Q), double mutants (E2785A/R2790A, E2847A/E2785A and E2847Q/E2795A), a transplanted M6 loop mutant and a deletion mutant (Δ2783–2790) were similarly generated, subcloned and expressed in *E. coli*. Cells were grown at 291 K after induction with 0.1 m*M* IPTG (isopropyl β-D-1-thiogalactopyranoside) for 20 h. Cells were harvested and suspended in lysis buffer consisting of 50 m*M* Tris–HCl pH 7.5, 500 m*M* NaCl, 1 m*M* PMSF (phenylmethylsulfonyl fluoride), 0.02%(*v*/*v*) β-mercaptoethanol, 10%(*v*/*v*) glycerol. After cell lysis by sonication, the His-tagged PTPRQ protein was purified by nickel-affinity chromatography. The PTPRQ protein was further purified by Q Sepharose ion-exchange chromatography and gel-filtration chromatography. The purified protein was dialyzed against a buffer consisting of 20 m*M* Tris–HCl pH 7.5, 0.2 *M* NaCl, 2 m*M* DTT, 10% glycerol and concentrated to 20 mg ml^{-1}.

2.2. Measurement of PTPRQ phosphatase activity

All PI analogues with a 1,2-dioctanoyl moiety attached at the D-1 position of the inositol ring were purchased from Cayman Chemical (Ann Arbor, Michigan, USA). Phosphatase activity was assayed by monitoring the amount of liberated phosphate ion using a malachite green colorimetric method. Lipid phosphatase assays were performed in a 80 µl reaction mixture consisting of 50 m*M* Tris–HCl pH 6.0, 10 m*M* DTT (dithiothreitol), 300 µ*M* PI(3,5)P_2 and 3 µg PTPRQ protein (wild type or mutant). The samples were incubated for 90 min at 310 K and the reaction was stopped by the addition of 20 µl malachite green/ammonium molybdate (1:1; 40 m*M* ammonium molybdate in 6 *N* HCl/1.5 m*M* malachite green containing 0.27% polyvinyl alcohol). The absorbance was measured at 650 nm using a plate reader. A standard curve for inorganic phosphate was generated for each assay. The same procedure was also used to measure the dephosphorylation of the phosphopeptide standards phosphoserinyl peptide (RRA-pS-PVA), PP2A peptide (KR-pT-IRR) and EGFR peptide (DADE-pY-LIPQQG). All kinetic experiments were performed at least in triplicate.

2.3. Measurement of pNPP dephosphorylation

Phosphatase activity was measured by monitoring the hydrolysis of *p*-nitrophenylphosphate (pNPP) using a spectrofluorometric assay. Reactions were performed in 50 m*M* Tris–HCl pH 6.0, 10 m*M* DTT, 1–50 m*M* pNPP with 3 µg of wild-type or mutant PTPRQ protein. The reaction mixture was incubated for 15 min and the reaction was stopped by the addition of 500 m*M* NaOH. Fluorescence emission was then detected at 405 nm in a fluorescence plate reader. The steady-state kinetics parameters K_m and k_{cat} were determined from a direct fit of the data to the Michaelis–Menten and the Lineweaver–Burk equations.

2.4. Crystallization

The C2879S mutant form was used for crystallization because the active-site cysteine is susceptible to oxidation. Because the His tag could not be removed by thrombin digestion during the purification step, crystallization trials were carried out using an *in situ* proteolysis method (Dong *et al.*, 2007). We confirmed that treatment with trypsin cleaved the thrombin-recognition site by determining the N-terminal sequence. The protein was concentrated to 20 mg ml^{-1},

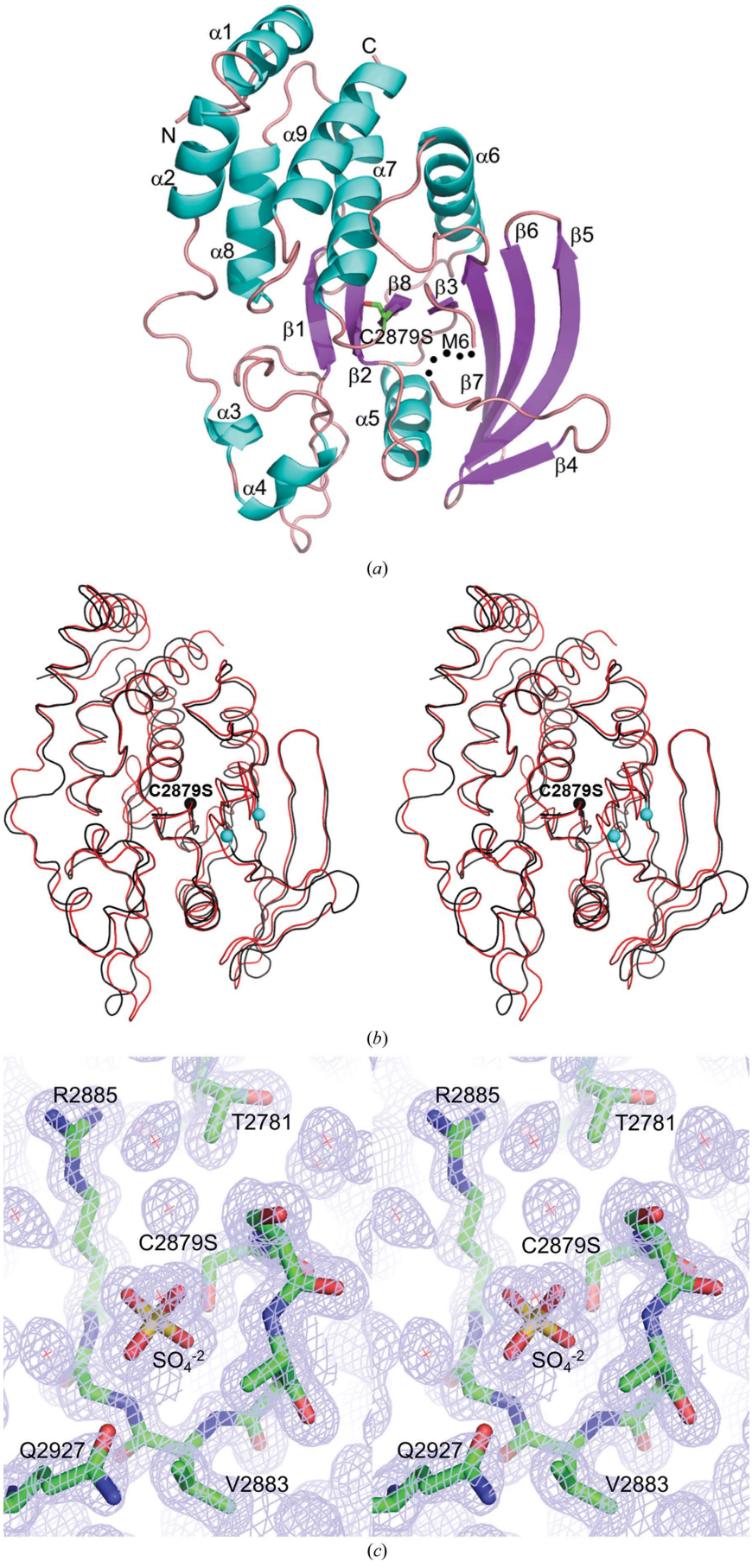

incubated with trypsin [1:100(*w*:*w*)] and screened for crystallization at 291 K using commercial screening kits (Hampton Research, USA). The best crystals were grown by mixing 1.5 µl protein solution and an equal volume of reservoir solution consisting of 0.1 *M* sodium citrate pH 5.6, 0.2 *M* sodium citrate, 0.4 *M* ammonium sulfate, 1.0 *M* lithium sulfate. The crystal diffracted X-rays to 3.2 Å resolution and belonged to space group $I4_132$, with unit-cell parameters $a = b = c = 163.3$ Å, $\alpha = \beta = \gamma = 90^\circ$. Although we successfully obtained a structural solution, the value of the *R* factor resisted falling below 35% and the electron densities of several loops were difficult to interpret during model refinement. We therefore tried a microseeding crystallization approach. Seed preparations were made by thoroughly crushing the initial crystals. Crystal screening was performed using 20-fold diluted seeds and PTPRQ-C supplemented with trypsin. The ratio of PTPRQ-C to trypsin was set to 100:1(*w*:*w*). The best crystals were grown by mixing 0.9 µl protein mixture solution with an equal volume of reservoir solution consisting of 0.2 *M* magnesium acetate, 0.1 *M* sodium citrate pH 5.6, 30% PEG 4K at 291 K.

2.5. Data collection, structure solution and refinement

X-ray diffraction data were collected on beamline 5A at the Photon Factory, Tsukuba, Japan. The crystal in the droplet was transferred to a cryosolution consisting of the mother liquor supplemented with 20%(*v*/*v*) ethylene glycol for 1 min and was flash-cooled in a nitrogen-gas stream at 93 K. The crystal diffracted to 1.56 Å resolution and belonged to space group $P6_4$, with unit-cell parameters $a = b = 77.58$, $c = 85.24$ Å, $\alpha = \beta = 90$, $\gamma = 120^\circ$. The collected diffraction data were processed

Figure 1
Crystal structure of PTPRQ-C. (*a*) Ribbon representation of PTPRQ-C. The side chain of the active-site C2879S is represented as a stick. The dotted line indicates the disordered M6 loop. (*b*) Structural comparison of PTPRQ-C and PTPδ. A worm trace of PTPRQ-C (black) is superimposed on that of PTPδ (red). The active-site C2879S is shown as a black sphere, whereas the positions of the disordered M6 loop boundaries are indicated as cyan spheres. (*c*) The $2F_o - F_c$ electron-density map around the active site superposed on the refined model. The map is contoured at the 1.0σ level.

Table 1
Data-collection and refinement statistics.

Values in parentheses are for the highest resolution bin.

Data collection	
Space group	$P6_4$
Unit-cell parameters (Å, °)	$a = b = 77.58$, $c = 85.24$, $\alpha = \beta = 90$, $\gamma = 120$
Resolution (Å)	40–1.56 (1.64–1.56)
Unique reflections/total reflections	41238/441545
Completeness (%)	99.8 (100.0)
$R_{\rm merge}$† (%)	4.8 (38.3)
$\langle I/\sigma(I)\rangle$	11.3 (2.0)
Refinement	
No. of reflections	41202
No. of atoms	2498
$R_{\rm cryst}/R_{\rm free}$	0.147/0.165
R.m.s. deviations	
Bond distances (Å)	0.013
Bond angles (°)	1.46
Dihedrals (°)	14.8
Temperature factors (Å^2)	
Wilson B factor	17.0
Protein atoms	22.3
Solvent atoms	32.1

† $R_{\rm merge} = \sum_{hkl}\sum_i |I_i(hkl) - \langle I(hkl)\rangle| / \sum_{hkl}\sum_i I_i(hkl)$, where $I_i(hkl)$ is the intensity of the ith measurement of an equivalent reflection with indices hkl.

and scaled using *MOSFLM* (Leslie, 1999) and *SCALA* (Winn *et al.*, 2011), respectively. The statistics of data collection and refinement are summarized in Table 1. The structure of PTPRQ-C was determined by the molecular-replacement method using the PTPRO structure (PDB entry 2gjt) as a search model (Barr *et al.*, 2009). *Phaser* (McCoy *et al.*, 2005) placed one monomer in the asymmetric unit of the crystal. Refinement was carried out using *PHENIX* (Adams *et al.*, 2010). A randomly selected 5% of the data were set aside for calculation of $R_{\rm free}$. Rounds of refinements were performed with manual rebuilding using *Coot* (Emsley & Cowtan, 2004). The final $R_{\rm cryst}$ and $R_{\rm free}$ were 14.7 and 16.5%, respectively. The model was validated using *MolProbity* (Chen *et al.*, 2010). A Ramachandran plot showed that 98.1 and 1.9% of all residues fell within the most favoured and additionally favoured regions, respectively, with no outliers. The all-atom clash score was 2.74 (99th percentile) and the *MolProbity* score was 1.49 (89th percentile). The final model included residues 2659–2783 and 2791–2939, one sulfate ion, one chloride ion and 284 water molecules. The figures were prepared using *PyMOL* (http://www.pymol.org).

3. Results and discussion

3.1. Structural description of the catalytic domain of PTPRQ

The crystal structure of the catalytic domain of PTPRQ (PTPRQ-C) was determined by the molecular-replacement method and refined to 1.56 Å resolution. The topological structure of PTPRQ-C comprises a central twisted eight-stranded β-sheet flanked by six α-helices (α1, α2 and α6–α9) on one face and three (α3–α5) on the other (Fig. 1*a*). A search for homologous structures using the *DALI* server (Holm & Sander, 1993) revealed that the closest was that of the catalytic domain of receptor-type PTPδ (PDB entry 2nv5, Z-score 39.7; Almo *et al.*, 2007). More than 240 classical PTP structures (29 unique members of classical PTP families) were identified with Z-scores greater than 30, indicating that PTPRQ adopts a fold that is very similar to those of other classical PTPs. When the PTPRQ-C structure was aligned with that of PTPδ, 264 out of 281 C^α atoms could be superposed with a root-mean-square deviation of 1.55 Å (Fig. 1*b*).

The most prominent differences were found in the α2–α3 loop and the β3–β6 loop (hereafter referred to as the M6 loop). The α2–α3 loop is located at the rim of a well known secondary phosphotyrosine-binding site in the crystal structure of PTP1B in complex with phosphorylated insulin receptor peptide (Salmeen *et al.*, 2000). The M6 loop is positioned near the catalytic core and constitutes a wall of the catalytic pocket. Notably, residues 2784–2790 in the M6 loop are disordered in the PTPRQ-C structure. In PTPδ, a short antiparallel β-hairpin lies between β3 and β6. These two β-strands extend the central β-sheet laterally and are positioned near the catalytic core, resulting in a deep catalytic pocket. Of 74 crystal structures of individual classical PTPs in the PDB, more than 75% adopt an ideal β-hairpin within the M6 loop (Critton *et al.*, 2011). Furthermore, the structures of only two PTPs, DEP1 (PDB entry 2cfv; Barr *et al.*, 2009) and HePTP (PDB entry 1zc0; Mustelin *et al.*, 2005), have been determined in the absence of structural information about the M6 loop.

The PTPRQ-C structure near the active site represents a conformation typical of those found in most classical PTPs (Fig. 1*c*). The amides of the main chain in the PTP loop strongly interact with the O atoms of the sulfate ion, which was incorporated as a crystallizing agent. The side chain of C2879S, which acts as a nucleophile, is ideally situated beneath the PTP loop. In contrast to other PTPs, the side chain of Arg2885 is stretched in an extended conformation without interacting with the sulfate ion. Instead, the guanidine group of Arg2885 interacts with Leu2779 *via* a hydrogen bond (Arg2885 NH2$\cdots$Leu2779 O; 2.9 Å). The WPE loop in PTPRQ-C adopts an open conformation with a position similar to that of the corresponding WPD loop in other classical PTPs. The average value of the thermal B factors for the residues including the WPE loop [the average B factor for residues 2845–2849 (WPEHG) is 43.3 Å^2] is high compared with those for other regions (the average B factor for the whole molecule is 22.3 Å^2), reflecting the flexible nature of this loop. PTPRQ-C exhibited optimal activity at pH 5.0, suggesting that the redox potential of PTPRQ-C is similar to those of other PTPs (Supplementary Fig. S1[1]).

3.2. A disordered M6 loop results in a flat catalytic pocket that could be suitable for PI substrates

The disordered nature of the M6 loop in PTPRQ might be caused by weak interactions between the M6 loop and the body of the molecule. In most classical PTPs, the M6 loop

[1] Supplementary material has been deposited in the IUCr electronic archive (Reference: DW5043). Services for accessing this material are described at the back of the journal.

makes several contacts with the main body of the catalytic domain. Firstly, Glu115 (PTP1B numbering; used hereafter) in the M6 loop makes bidentate hydrogen bonds to the side chain of Arg221. A mutation of Glu115 to alanine in PTP1B has been shown to result in a 100-fold decrease in the k_{cat} value (Zhang, 2002). Secondly, Lys122 in the M6 loop contacts Asp181 in the WPD loop. Finally, the highly conserved Tyr48 in the M1 loop directs the side chain of Ser216 in the PTP loop outside the active-site pocket; Ser216, in turn, forms a hydrogen bond to the main-chain O atom of Lys120 in the M6 loop. In PTPRQ, the residues corresponding to Lys120 and Asp181 are changed to arginine and glutamate, respectively; Tyr48 is also changed to phenylalanine. These changes might cause the relevant residues to deviate from the ideal geometry necessary to form hydrogen bonds, thereby contributing to disruption of the interactions between the M6 loop and the body of the catalytic domain. The disordered M6 loop results in the catalytic pocket being flat on one side, which is an unusual characteristic for a classical PTP.

The atypical (for classical PTPs) flat catalytic pocket of PTPRQ-C led us to test whether this property is a determinant of the catalytic activity towards PI substrates. Among cysteine-based PTPs that are capable of dephosphorylating PIs (PTEN, TPIP, MTMR and tensin), human PTEN (Lee *et al.*, 1999), human MTMR (Begley *et al.*, 2003), the *Ciona intestinalis* PTEN homologue (Matsuda *et al.*, 2011) and PTPMT1 (Xiao *et al.*, 2011) have been characterized structurally. Of these, the structures of MTMR2 and PTPMT1 have been characterized in complex with a PI substrate (Begley *et al.*, 2006; Xiao *et al.*, 2011). To explore the structural origin of the PI substrate-dephosphorylating activity, we superimposed the structure of PTPRQ-C on those of PTP1B, a prototypical classical PTP that exclusively dephosphorylates pTyr substrates, and MTMR2, which is capable of dephosphorylating PI(3,5)P_2, in complex with PI(3,5)P_2. The superposition (Figs. 2*a* and 2*b*) shows that the residues of the M6 loop in PTP1B clash with the diacyl moiety of PI(3,5)P_2 in the MTMR2 structure, suggesting that the flat catalytic pocket caused by disorder of the M6 loop might be responsible for the specificity of PTPRQ for PI substrates.

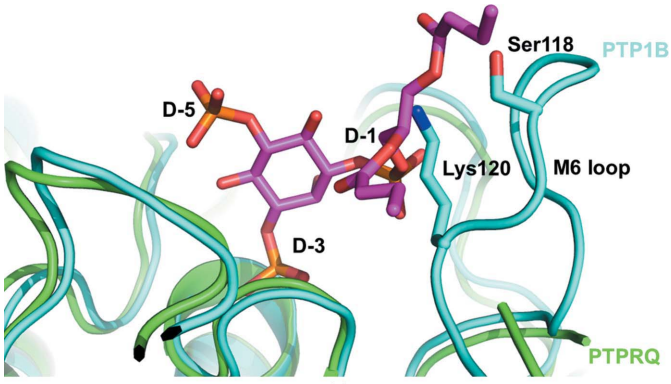

Figure 2
Superposition of the PTPRQ-C structure (apo form) with those of PTP1B and of MTMR2 in complex with PI(3,5)P_2. (*a*) Worm traces of PTPRQ-C (green) and PTP1B (cyan) are shown. The bound PI(3,5)P_2 in MTMR2 is shown for clarity. (*b*) Comparison of the active-site surface of PTPRQ-C (orange) with those of PTP1B (green) and MTMR2 (blue). PI(3,5)P_2 bound to MTMR2 is shown as black sticks.

3.3. PTPRQ displays dephosphorylating activity towards PI substrates

To explore the substrate specificity of PTPRQ, we first tested wild-type and CS mutant PTPRQ-C against various substrates, including monophosphorylated synthetic peptides (phosphoserinyl, phosphothreonyl and phosphotyrosyl peptides) and diC8-PI(3,4,5)P_3 (Supplementary Material). Whereas the wild-type PTPRQ-C displayed Michaelis–Menten kinetics, the CS mutant form did not, suggesting that the catalytic activity originates with the active-site cysteine residue. PTPRQ-C displayed strong activity towards PI(3,4,5)P_3 but not towards phosphoserinyl, phosphothreonyl or phosphotyrosyl peptides, indicating that PTPRQ-C has a preference for PI substrates (Supplementary Fig. S2).

To further elucidate the substrate specificity of PTPRQ, we tested its catalytic activity towards all PI substrates (Fig. 3). It has previously been reported that GST-fused PTPRQ from rat possesses a relatively broad specificity for PIs, but exhibits prominent activity towards PI(3,5)P_2 and PI(4,5)P_2 (Oganesian *et al.*, 2003). In contrast, we found that human PTPRQ displayed a strong preference for the substrate PI(3,4,5)P_3. It also displayed significant activity towards

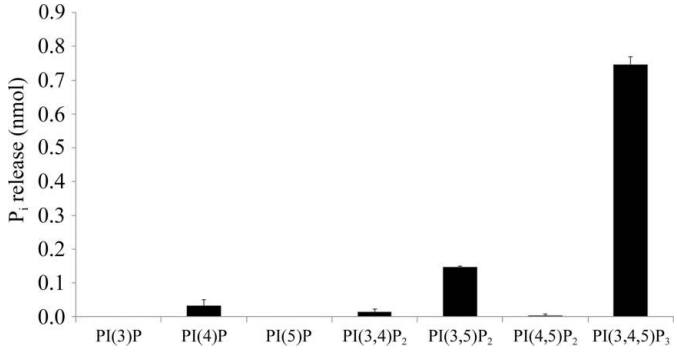

Figure 3
Catalytic activity of PTPRQ-C toward various substrates. PTPRQ shows a strong preference for PI(3,4,5)P_3 over other PIPs.

Table 2
Kinetic data of PTPRQ-C variants for the hydrolysis of pNPP and $PI(3,4,5)P_3$.

	pNPP			PI(3,4,5)P3
Enzyme	K_m (m*M*)	k_{cat} (min^{-1})	k_{cat}/K_m (min^{-1} mM^{-1})	P_i release (nmol)
WT	1.966	0.277	0.143	0.712
ΔM6	4.520	0.026	0.006	0.403
EARA	1.767	0.058	0.033	0.241
E2785A	2.352	0.049	0.023	0.267
R2790A	1.901	0.189	0.100	0.149
WPQ	1.050	0.061	0.060	0.611
WPA	0.933	0.102	0.115	1.391
WPA-EA	0.522	0.062	0.119	0.000
WPQ-EA	0.630	0.052	0.086	0.012
CS	—	—	—	0.009

$PI(3,5)P_2$, but showed no measurable activity against the remaining PIP analogues. This might suggest that PTPRQ has the potential to exhibit high selectivity among the wide variety of PI substrates.

3.4. Effects of M6 loop deletion or destabilizing mutations on *in vitro* catalytic activity

To test whether the flat catalytic pocket of PTPRQ is correlated with the dephosphorylating activity towards PI substrates, we generated a series of PTPRQ-C mutants, including those that potentially destabilize the contact with the active site (E2785A), the binding of PTPRQ-C to PI substrates (R2790A) or both (E2785A/R2790A double mutant; EARA); we also completely deleted the M6 loop (residues 2783–2790; ΔM6). The R2790A mutation was introduced because superposition of PTP1B and complexed MTMR2 showed that Arg2790 can potentially contribute to binding to the D-1 phosphate of PIP substrates (Begley *et al.*, 2006). The active-site cysteine mutant C2879S was also included as a negative control. To simply evaluate dephosphorylation ability, we first monitored the catalytic activities of the mutants using pNPP substrate (Table 2). pNPP, the most widely used substrate for PTPs, can be hydrolyzed without an appropriate general acid and is thus particularly suitable for this case (McCain *et al.*, 2004). With the exception of the R2790A mutation, all of the mutations resulted in a significant decrease in catalytic activity towards pNPP substrate. This was especially notable for the ΔM6 and E2785A mutants, in which the activity towards pNPP was reduced by ∼80 and ∼90%, respectively. As is the case for PTP1B (Guo *et al.*, 2002), the R2790A mutant of PTPRQ-C retained ∼70% of the catalytic activity of wild-type PTPRQ-C. These results show that the M6 loop is still necessary for dephosphorylation of pNPP even when it is disordered in the crystal.

We next tested the catalytic activities of wild-type PTPRQ and its mutants towards the $PI(3,4,5)P_3$ substrate, which we found to be the optimal substrate for PTPRQ. In contrast to the results obtained using the pNPP substrate, the ΔM6 loop mutant showed intrinsic, albeit reduced, activity towards $PI(3,4,5)P_3$ (Table 2). The E2785A mutant, which exhibited significantly altered pNPP dephosphorylation, displayed a catalytic efficiency towards $PI(3,4,5)P_3$ that was approximately one-third of that of wild-type PTPRQ. Also unlike the results obtained using the pNPP substrate, the R2790A mutation resulted in an approximately 80% decrease in the dephosphorylating activity, indicating that Arg2790 might play a role in dephosphorylating the $PI(3,4,5)P_3$ substrate. It appeared that PI substrate binding to PTPRQ-C might induce a conformational rearrangement of the M6 loop. Overall, these data suggest that M6 loop-destabilizing mutations severely compromise the dephosphorylating activity of PTPRQ for pNPP while mildly decreasing its catalytic activity towards the substrate $PI(3,4,5)P_3$.

Table 3
Kinetic data of PTPRQ-C mutants (WPD, M6 and dual mutant) for the hydrolysis of pNPP and $PI(3,4,5)P_3$.

	pNPP			$PI(3,4,5)P_3$
Enzyme	K_m (m*M*)	k_{cat} (min^{-1})	k_{cat}/K_m (min^{-1} mM^{-1})	P_i release (nmol)
WT	1.966	0.277	0.143	0.712
WPD	1.740	4.830	2.811	0.006
WPD-M6	1.688	4.053	2.401	0.062
M6	1.213	0.087	0.074	0.766

To further confirm whether the specificity for PI substrates caused by the characteristics of the M6 loop residues of PTPRQ or the weak contact of the M6 loop with the body of the molecule originates from the change from WPD to WPE, we introduced three mutations. Firstly, we generated a hybrid containing the M6 loop transplanted from PTP1B (FEKGRIR for PTPRQ-C; MEKGSLK for PTP1B). Secondly, we mutated WPE to WPD in PTPRQ. Thirdly, we made a dual-mutant hybrid of PTP1B and WPD. The hybrid mutant showed decreased catalytic activity towards pNPP but unchanged activity towards $PI(3,4,5)P_3$, suggesting that the sequence in the M6 loop might not be the determinant of the PI substrate specificity (Table 3). However, the WPD mutant form showed a marked increase (∼20-fold) in catalytic activity towards pNPP but no measurable activity towards $PI(3,4,5)P_3$. The dual mutation also produced results similar to those for the WPD mutation, suggesting that a WPD to WPE change might disrupt the interactions between the M6 loop and the body of the catalytic domain, with a concomitant change in substrate specificity.

3.5. Exploring the role of a general acid residue in the dephosphorylation of PIP substrates

As noted in §1, PTPRQ has a glutamate instead of an aspartate in the WPD motif. To examine whether this glutamate functions as a general acid, we mutated it to alanine (E2847A) or glutamine (E2847Q) and tested the activities of the resulting mutants (Table 2). Whereas the E2847Q mutant displayed catalytic activity comparable to that of wild-type PTPRQ, the catalytic activity of the E2847A mutant was increased by twofold. This result suggests the possibility that PTPRQ does not require a general acid for catalysis. Apart from the glutamate residue in the WPE loop, the only

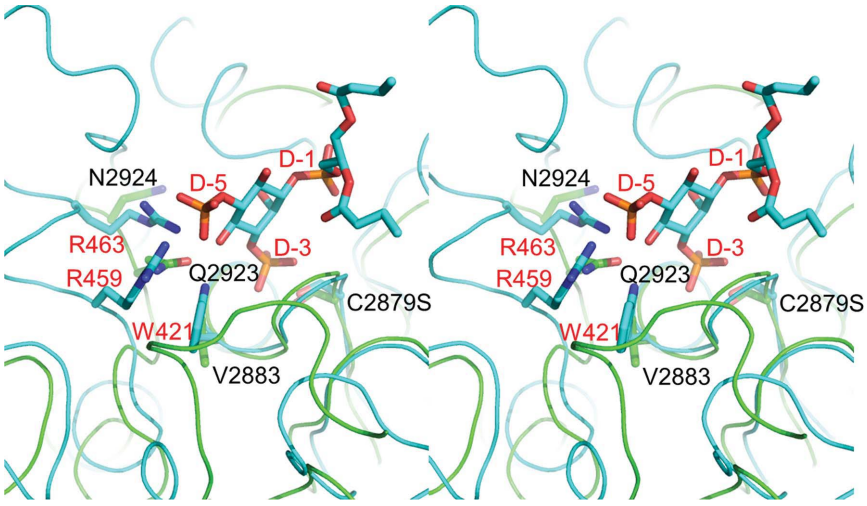

Figure 4
The structural basis for the substrate specificity for PI(3,4,5)P_3. A worm model of PTPRQ is superposed with that of MTMR2 in complex with PI(3,5)P_2. Residues involved in the interaction with PI(3,5)P_2 are shown labelled in black (PTPRQ-C) and red (MTMR2).

candidate for a general acid in the PTPRQ-C structure is Glu2785, which when mutated substantially reduces but does not abolish activity towards PI(3,4,5)P_3. Two double mutations, E2785A/E2847A (WPA-EA) and E2785A/E2847Q (WPQ-EA), showed no measurable activity towards PI(3,5)P_2, implying that dephosphorylation of PI(3,4,5)P_3 preferentially proceeds through an unprecedented general acid, Glu2785, in the M6 loop of PTPRQ. Taken together, these data suggest that a glutamate in the WPE loop is not a prerequisite for dephosphorylating PI(3,4,5)P_3.

3.6. Hypothetical model of the strong preference for PI(3,4,5)P_3

MTMR phosphatase can dephosphorylate the phosphate group at the D-3 position in either PI(3,5)P_2 or PI(3)P but not in PI(3,4,5)P_3. As shown in Fig. 4, the side chain of Trp421 in MTMR2 makes contact with a hydroxyl group at the D-4 position in PI(3,5)P_2 [Trp421 NE1$\cdots$PI(3,4,5)P_3 O4; 2.8 Å], precluding access of PI(3,4,5)P_3 to the active site of MTMR2. However, the residue corresponding to Trp421 in MTMR2 is changed to valine, which might provide sufficient space to accommodate the incoming PI(3,4,5)P_3. Furthermore, Gln2923 and Asn2924 potentially interact with a phosphate group at the D-5 position of the substrate. The structural superposition shown here supports our hypothesis that PTPRQ has a substrate-recognition pattern similar to that of MTMR. Moreover, these results are consistent with the fact that overexpression of the cytoplasmic version of PTPRQ markedly reduces Akt/PKB signalling, which is regulated by the level of PI(3,4,5)P_3 (Oganesian *et al.*, 2003).

4. Conclusions

In summary, we have determined the crystal structure of PTPRQ-C at 1.56 Å resolution. The crystal structure of PTPRQ-C presented here shows an active-site pocket that is flat on one side owing to disorder of the M6 loop. The M6-loop disorder involves several nonconserved residues, especially those in the WPE motif, and results in weak contact between the residues of the active site and the M6 loop. Guided by the superposition of PTPRQ-C with the structure of MTMR2 in complex with PI(3,5)P_2, our subsequent kinetic experiments using wild-type and mutant PTPRQ-C showed that a flat active site is important for the dephosphorylation of PIP substrates. Further, we demonstrated that PTPRQ has a strong preference for PI(3,4,5)P_3, suggesting that PTPRQ plays a role in the negative regulation of Akt signalling. The atomic coordinates and structural parameters of the final structure have been deposited in the Protein Data Bank (PDB) with code 4ikc.

The authors are grateful to the staff of beamline 5A at the Photon Factory and of beamline 4A at Pohang Accelerator Laboratory for help with diffraction experiments. This work was supported by grants from the National Research Foundation of Korea (NRF; 2011-0030027) and the World Class Institute (WCI) Program of the NRF (WCI 2009-002) funded by the Korean Government Ministry of Education Science and Technology (MEST).

References

Adams, P. D. *et al.* (2010). *Acta Cryst.* D**66**, 213–221.
Almo, S. C. *et al.* (2007). *J. Struct. Funct. Genomics*, **8**, 121–140.
Alonso, A., Sasin, J., Bottini, N., Friedberg, I., Friedberg, I., Osterman, A., Godzik, A., Hunter, T., Dixon, J. & Mustelin, T. (2004). *Cell*, **117**, 699–711.
Andersen, J. N., Mortensen, O. H., Peters, G. H., Drake, P. G., Iversen, L. F., Olsen, O. H., Jansen, P. G., Andersen, H. S., Tonks, N. K. & Møller, N. P. (2001). *Mol. Cell. Biol.* **21**, 7117–7136.
Barford, D., Flint, A. J. & Tonks, N. K. (1994). *Science*, **263**, 1397–1404.
Barr, A. J., Ugochukwu, E., Lee, W. H., King, O. N., Filippakopoulos, P., Alfano, I., Savitsky, P., Burgess-Brown, N. A., Müller, S. & Knapp, S. (2009). *Cell*, **136**, 352–363.

Begley, M. J., Taylor, G. S., Brock, M. A., Ghosh, P., Woods, V. L. & Dixon, J. E. (2006). *Proc. Natl Acad. Sci. USA*, **103**, 927–932.
Begley, M. J., Taylor, G. S., Kim, S. A., Veine, D. M., Dixon, J. E. & Stuckey, J. A. (2003). *Mol. Cell*, **12**, 1391–1402.
Chen, V. B., Arendall, W. B., Headd, J. J., Keedy, D. A., Immormino, R. M., Kapral, G. J., Murray, L. W., Richardson, J. S. & Richardson, D. C. (2010). *Acta Cryst.* D**66**, 12–21.
Critton, D. A., Tautz, L. & Page, R. (2011). *J. Mol. Biol.* **405**, 619–629.
Dong, A. *et al.* (2007). *Nature Methods*, **4**, 1019–1021.
Emsley, P. & Cowtan, K. (2004). *Acta Cryst.* D**60**, 2126–2132.
Goodyear, R. J., Jones, S. M., Sharifi, L., Forge, A. & Richardson, G. P. (2012). *J. Neurosci.* **32**, 2762–2772.
Guo, X.-L, Shen, K., Wang, F., Lawrence, D. S. & Zhang, Z.-Y. (2002). *J. Biol. Chem.* **277**, 41014–41022.
Holm, L. & Sander, C. (1993). *J. Mol. Biol.* **233**, 123–138.
Jia, Z., Barford, D., Flint, A. J. & Tonks, N. K. (1995). *Science*, **268**, 1754–1758.
Lee, J.-O., Yang, H., Georgescu, M.-M., Di Cristofano, A., Maehama, T., Shi, Y., Dixon, J. E., Pandolfi, P. & Pavletich, N. P. (1999). *Cell*, **99**, 323–334.
Leslie, A. G. W. (1999). *Acta Cryst.* D**55**, 1696–1702.
Matsuda, M., Takeshita, K., Kurokawa, T., Sakata, S., Suzuki, M., Yamashita, E., Okamura, Y. & Nakagawa, A. (2011). *J. Biol. Chem.* **286**, 23368–23377.
McCain, D. F., Grzyska, P. K., Wu, L., Hengge, A. C. & Zhang, Z.-Y. (2004). *Biochemistry*, **43**, 8256–8264.
McCoy, A. J., Grosse-Kunstleve, R. W., Storoni, L. C. & Read, R. J. (2005). *Acta Cryst.* D**61**, 458–464.
Mustelin, T., Tautz, L. & Page, R. (2005). *J. Mol. Biol.* **354**, 150–163.
Oganesian, A., Poot, M., Daum, G., Coats, S. A., Wright, M. B., Seifert, R. A. & Bowen-Pope, D. F. (2003). *Proc. Natl Acad. Sci. USA*, **100**, 7563–7568.
Salmeen, A., Andersen, J. N., Myers, M. P., Tonks, N. K. & Barford, D. (2000). *Mol. Cell*, **6**, 1401–1412.
Seifert, R. A., Coats, S. A., Oganesian, A., Wright, M. B., Dishmon, M., Booth, C. J., Johnson, R. J., Alpers, C. E. & Bowen-Pope, D. F. (2003). *Exp. Cell Res.* **287**, 374–386.
Tonks, N. K. (2006). *Nature Rev. Mol. Cell Biol.* **7**, 833–846.
Winn, M. D. *et al.* (2011). *Acta Cryst.* D**67**, 235–242.
Xiao, J., Engel, J. L., Zhang, J., Chen, M. J., Manning, G. & Dixon, J. E. (2011). *Proc. Natl Acad. Sci. USA*, **108**, 11860–11865.
Zhang, Z.-Y. (2002). *Annu. Rev. Pharmacol. Toxicol.* **42**, 209–234.